





Development of geometry-driven quantitative prediction for shrinkage porosity in T-junction of steel sand castings

Kamar Mazloun ^{*1}, Amit Sata ¹

¹ Marwadi University, Department of Mechanical Engineering, India, kamar.mazloun112219@marwadiuniversity.ac.in, amit.sata@marwadieducation.edu.in

Cite this study:

Mazloun, K., & Sata, A. (2024). Development of geometry-driven quantitative prediction for shrinkage porosity in T-junction of steel sand castings. *Turkish Journal of Engineering*, 8 (4), 640-646.

<https://doi.org/10.31127/tuje.1454237>

Keywords

Shrinkage porosity
Plain carbon steel
Casting simulation
Sand casting
Criterion function

Research/Review Article

Received: 17.03.2024
Revised: 01.04.2024
Accepted: 17.04.2024
Published: 31.10.2024



Abstract

Shrinkage porosity poses a significant challenge in metal casting processes, impacting both productivity and energy efficiency, especially when dealing with components that are not accepted or reprocessed. Addressing this issue requires proactive measures, and predictive techniques play a crucial role in minimizing its occurrence. Among these methods, the Criterion Function stands out as a valuable empirical model extensively explored in the literature. By intricately linking solidification processes to the development of shrinkage porosity, the Criterion Function leverages key process parameters, including thermal gradient, molten metal velocity during solidification, and cooling rate, to offer predictive insights into the location and presence of porosity. However, a criterion function is needed that also considers the effect of geometric variations as well as the size of the defect (shrinkage porosity). In this study, a casting with three T-joints was taken as a benchmark shape to develop a geometry-based quantitative prediction model for plain carbon steel castings. Real experimental results were combined with solidification simulation results to produce reliable data, which were then used to extrapolate the results. The developed quantitative prediction model, which includes the effect of geometric changes, has been validated and proven effective in predicting shrinkage porosity.

1. Introduction

Plain carbon steel is economically efficient, strong, and durable, making it ideal for industrial casting [1,2]. This allows for the production of a wide variety of components. The formation of porosity resulting from solidification shrinkage, or shrinkage porosity, is an important issue in the industrial casting business. It is typically viewed as unsatisfactory because it adversely affects the mechanical qualities of cast components [3-5]. In order to ensure the quality of plain carbon steel parts, shrinkage porosity must be handled, necessitating effective solutions for high-quality manufacturing procedures. Shrinkage porosity appears in the final phase of solidification, where the reduction in the central matrix's volume cannot be fully compensated by molten steel flowing in from upstream, primarily due to a high

solid fraction [6]. During the solidification process, identifying a generated liquid phase isolated region in the casting allows for the preliminary determination of both its location and potential defects. Subsequently, predictions about the location and size of defects can be made post-solidification [7,8]. Analyzing the temperature distribution during the filling and solidification of liquid metal enables anticipating defect locations and provides insights to improve the manufacturing process [9]. The casting production process is complex, and the quality of the final product depends on various process parameters. Currently, metal foundries largely rely on a "trial and error" approach in their design, with casting designers' expertise playing a significant role in ensuring quality and minimizing potential errors. Achieving optimal results for casting parameters is challenging through traditional

mathematical calculations [10-12]. To achieve high-quality casting, it is essential to experimentally control casting parameters or utilize engineering and production systems such as Computer-Aided Simulation (CAS) [13,11]. Casting simulation proves to be a highly effective strategy for preventing shrinkage porosity in metal castings, contributing to lower rejection rates, decreased energy loss, and enhanced productivity in foundries [14]. In the last two decades, the application of casting simulation and numerical methods has gained popularity with the advancement of powerful computing facilities. This method involves solving governing equations representing various physical phenomena in metal casting, such as flow, heat transfer, solidification, phase transformation, and stress/strain formation [15]. While statistical and artificial intelligence-based techniques have been employed for defect prediction [16], their widespread adoption is limited due to the challenges associated with extensive data collection.

In a series of separate investigations concentrating on predicting defects in casting processes, various advanced techniques using numerical methods are explored to forecast different types of defects. One study specifically explores the application of Darcy's Equation to predict the occurrence of shrinkage and gas porosity [17]. Another approach, like the Finite Element Method (FEM), is employed because it can simulate various structural elements [18]. For instance, one investigation utilizes FEM to anticipate porosity distribution, considering factors like exothermic powder, chills, and pads [19]. Another paper investigates metal flow through finite element analysis, using the continuity equation to prevent casting defects such as porosity and air entrainment [20]. A separate study employs modeling methods to analyze the impact of varying conditions on molten fluidity, particularly assessing the filling stage during casting [21]. Another investigation establishes a method for predicting the fraction and distribution of micro porosity [22]. For example, one of these studies utilizes a mushy-zone refinement technique to predict pipe shrinkage, macro porosity, and micro porosity [23]. The Volume of Fluid (VOF) approach is utilized in a different study to predict the formation and shape of shrinkage [24]. Furthermore, effective prediction of the volumetric fraction of porosity resulting from hydrogen gas precipitation in plate casting is demonstrated [25]. Lastly, a distinct study extends its predictive capabilities to the development of shrinkage in alloys characterized by both short and lengthy freezing ranges [26]. Together, these varied studies offer valuable insights into defect prediction, presenting a comprehensive approach to foresee and address various casting defects.

Casting simulation relies heavily on criterion functions, derived essentially from thermal parameters [27]. These functions are obtained by solving governing equations through suitable numerical methods to forecast the occurrence of shrinkage porosity. The utilization of these criterion functions is notably advantageous, given their ease of integration with casting simulation tools and the straightforward interpretation of results. Table 1 provides a compilation of assorted criterion functions used for particular metallic alloys.

Criterion functions, recognized for their effectiveness, have been developed in recent years to forecast the occurrence of shrinkage porosity, primarily addressing thermal parameters within specific process-alloy combinations. However, further exploration is needed to assess both the quantity of shrinkage porosity and the geometric influence on shrinkage porosity.

Table 1. The assorted criterion functions [28].

| Criterion Function | Bishop | Davies | Khan | Niyama | Lee | St Kao |
|---|------------|--------|------|--------|----------|--------|
| Year | 1951 | 1975 | 1980 | 1982 | 1990 | 1994 |
| a | 1 | 1 | 0 | 1 | 1 | 0.38 |
| Model: $\frac{G^a \times t_s^d}{v_s^b \times R^c}$ | b | 0 | -1 | 0 | -1 | - |
| c | 0 | 0 | 0 | -0.5 | 0 | 0 |
| d | 0 | 0 | 0 | 0 | 2/3 | 0 |
| Remarks | Cast Steel | -- | -- | Steel | Al alloy | -- |

Nomenclature: R: Cooling rate, v_s : Solidification velocity, t_s : local solidification time, G: Temperature gradient

2. Selection of a benchmark shape

Variations in the shape of metal castings influence the location and size of shrinkage porosity. In the development of an empirical model for predicting shrinkage porosity, selecting a standard form became necessary. Castings with a junction shape are often associated with a higher likelihood of developing shrinkage porosity [29]. Consequently, the T-junction shape was chosen as the benchmark, combining three T-junctions, as illustrated in Figure 1. The benchmark shape encompasses four cases of stem thickness, each with three different values of stem length, resulting in a total of 12 designs, as appeared in Table 2. The dimensions of the casting's depth, total length, and arm thickness remained constant. However, to investigate the impact of geometry on porosity formation, two ratios related to arm thickness were considered: the thickness ratio R_1 (arm thickness to stem thickness) and the length ratio R_2 (arm thickness to stem length). The arm length was intentionally selected to ensure feeding independence, preventing solidification in one junction from affecting the other two. In all cases, the angle formed by the arm and stem remains a constant 90 degrees in sectional orientation. For this study, it is presumed that the arm and stem have zero radius.

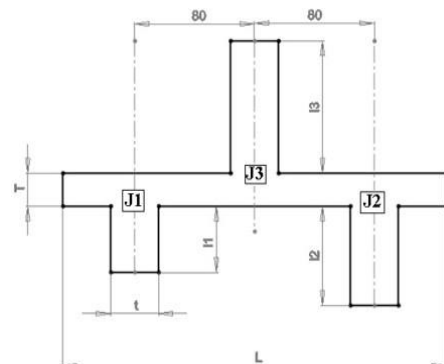


Figure 1. A benchmark shape combining three T-junctions.

Table 2. The dimensions pertaining to the benchmark casting.

| Case No | Thickness | | Depth (d) mm | Length | | | |
|---------|-------------|------------|--------------|---------------------------|---------------------------|---------------------------|--------------|
| | Stem (T) mm | Arm (t) mm | | Stem (I ₁) mm | Stem (I ₂) mm | Stem (I ₃) mm | Total (L) mm |
| 1 | 5 | | | | | | |
| 2 | 10 | | | | | | |
| 3 | 20 | 20 | 40 | 40 | 60 | 80 | 240 |
| 4 | 30 | | | | | | |

3. Geometry-Influenced criterion function development methodology

Current methods for predicting shrinkage porosity primarily focus on solidification-related factors, such as alloy temperature gradient and cooling rate. Numerous researchers have established correlations between these parameters and shrinkage porosity occurrence. Developing a criterion function to predict shrinkage porosity for a specific alloying process that considers the geometry effect requires collecting information not only about geometric parameters but also about temperature gradient and cooling rate during solidification.

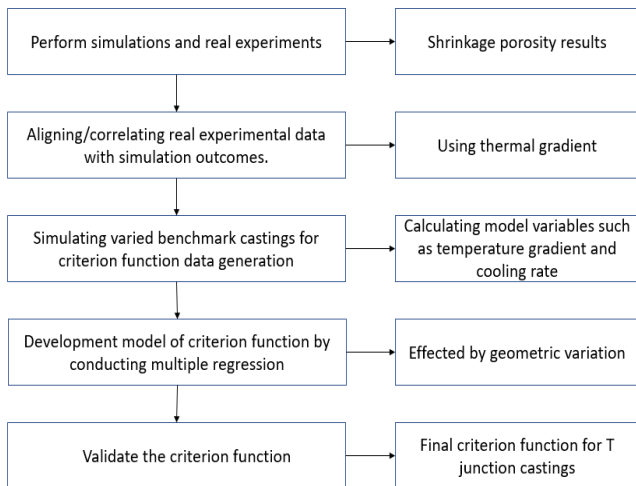


Figure 2. The technique employed in developing a geometry-influenced criterion function.

This information is typically obtained through numerical solutions or experiments. While numerical solutions demand precise boundary conditions for accuracy, obtaining real-time parameters during experiments poses significant challenges. Hence, an integrated approach is adopted for leveraging both numerical methods and experimental data to comprehensively understand solidification phenomena. Figure 2 illustrates this process, followed by a detailed step-by-step discussion of the methodology.

4. Simulations and experiments setup

Since large-scale cast-steel goods made of plain carbon steel are widely utilized in industry, this metal has been chosen as cast metal. Wide-ranging industries, including power generation, construction, transportation, and autos [30], have used large-scale cast steel products as essential structural elements. Table 3 lists the elements that make up plain carbon steel.

Table 3. Plain Carbon Steel elements (courtesy: regional industrial sand-casting foundry).

| Carbon | Silicon | Manganese | Phosphorus and Sulphur | Iron |
|---------|---------|-----------|------------------------|----------------|
| 0.045 % | 0.48 % | 0.85 % | Less than 0.09 % | More than 98 % |

4.1. Simulations

The simulation for all cases of the benchmark shape mentioned in Table 2 was conducted for the solidification process using casting simulation software developed based on fundamentals of Vector Element Method (VEM) which has been elaborately discussed in several technical literatures [31, 32]. This method is relatively quick in providing simulated results in comparison with other methods. The simulations were carried out with a mesh size of 0.5 mm. Simulation of the plain carbon steel solidification is depicted in Figure 3. The occurrence of shrinkage porosity can be predicted in the solidification process through transient thermal analysis with the application of appropriate initial and boundary conditions. The initial mold temperature was set to 27 °C, and the pouring temperature to 1657 °C. The Interfacial heat transfer coefficient for plain carbon steel to silica sand mold is taken as 570 W/m² K, and for the mold to the surrounding air, it is 11.2 W/m² K, assumed to be constant throughout solidification. The silica sand has a density of 1490 kg/m³ and exhibits a thermal conductivity of 0.519 W/m K and a specific heat of 1170 J/kg. Simulated results suggest that the benchmark shape may develop shrinkage porosity if a feeder is not provided during experiments.



Figure 3. Simulation of the plain carbon steel solidification.

4.2. Experiments

All variations in the benchmark shape were tested through experiments. For each variation in the benchmark form, two castings were made under identical conditions to account for any uncertainties.

Table 4. Particulars regarding the experiment.

| | |
|------------------------------|---------------------------------------|
| Molding box dimensions | 340 × 340 × 125 [mm] |
| Number of mold boxes | two |
| Pouring basin specifications | Square c/s 50 [mm] |
| Sprue dimensions | Cylinder: 25 [mm] Height: 125 [mm] |
| Rectangular gate dimensions | 25 × 10 [mm] |
| Number of gates | two |
| Number of cavities | Double |

Figure 4 illustrates the use of silica-based sand to create castings in green sand molds. Simple wood was utilized to craft the patterns, and to enhance the surface

smoothness of benchmark castings, wooden templates were painted with oil paint. After heating the metal to 1657 °C in an induction furnace, it was poured under gravity. Table 4 displays the specific details of the experiment setup.

Table 5. shrinkage porosity across all junctions.

| Junction | Data | Case 1 | Case 2 | Case 3 | Case 4 |
|-----------------------------------|---|---------|----------|----------|----------|
| 1 | R_1 = $\frac{\text{Stem thickness}}{\text{Arm thickness}}$ | 0.25 | 0.5 | 1 | 1.5 |
| | R_2 = $\frac{\text{Stem length}}{\text{Arm thickness}}$ | 2 | 2 | 2 | 2 |
| | Porosity [cm ³] | 0.1 | 0.2 | 1.6 | 2.5 |
| | Nomenclature [mm] (T – t – I ₁ , I ₂ , I ₃) | 20-5-40 | 20-10-40 | 20-20-40 | 20-30-40 |
| 2 | R_1 = $\frac{\text{Stem thickness}}{\text{Arm thickness}}$ | 0.25 | 0.5 | 1 | 1.5 |
| | R_2 = $\frac{\text{Stem length}}{\text{Arm thickness}}$ | 3 | 3 | 3 | 3 |
| | Porosity [cm ³] | 0 | 2.2 | 2.3 | 2.5 |
| | Nomenclature [mm] (T – t – I ₁ , I ₂ , I ₃) | 20-5-60 | 20-10-60 | 20-20-60 | 20-30-60 |
| 3 | R_1 = $\frac{\text{Stem thickness}}{\text{Arm thickness}}$ | 0.25 | 0.5 | 1 | 1.5 |
| | R_2 = $\frac{\text{Stem length}}{\text{Arm thickness}}$ | 4 | 4 | 4 | 4 |
| | Porosity [cm ³] | 0 | 0 | 0.1 | 0.45 |
| | Nomenclature [mm] (T – t – I ₁ , I ₂ , I ₃) | 20-5-80 | 20-10-80 | 20-20-80 | 20-30-80 |
| Casting Volume [cm ³] | | 228 | 264 | 336 | 408 |

To assess the presence of shrinkage porosity, benchmark castings were sliced both longitudinally and horizontally, 20 mm from the top surface. The primary goal of this section is to measure the volume of formed shrinkage porosity. Furthermore, by developing a quantitative model related to geometric influence, the study explores the impact of thermal parameters such as temperature gradient and rate of cooling, in conjunction with geometry, to estimate the magnitude of shrinkage porosity.

As shown in Table 5, the trials resulted in shrinkage porosity at various junctions, where the volume of water within the cavity determined the measurement of shrinkage porosity for each junction. To estimate the volume of shrinkage porosity in the castings, a medical syringe with a minimum increment of 0.1 ml was used to

inject a known amount of water into the voids formed through shrinkage porosity. According to experimental findings, the primary factors influencing the production of shrinkage porosity are thickness ratio and length ratio. It is evident that the formation of shrinkage porosity was greater at junction 2 compared to the other junctions.

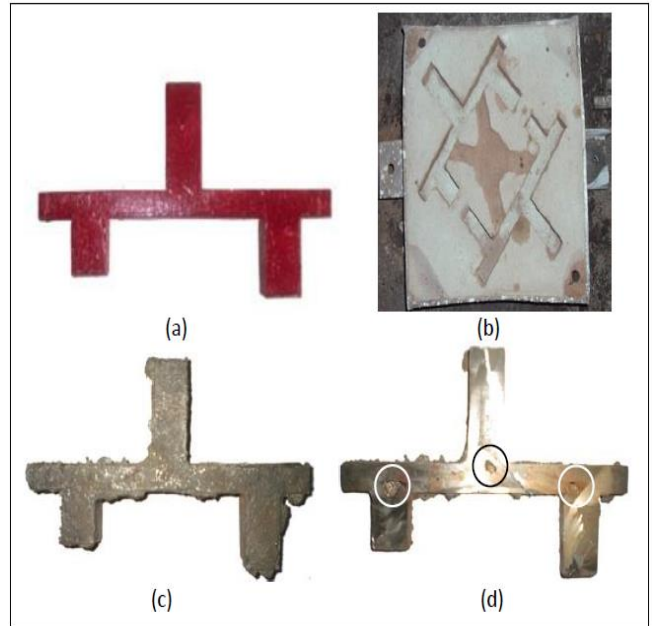


Figure 4. Experimental procedure: a) pattern of casting, b) mold, c) the cast product, d) cross-section in the casting.

5. Aligning/correlating real experiments with simulation:

The simulation tool is linked to the experimental results to obtain better and more reliable results, enabling us to develop a reliable experimental model that predicts the quantity of shrinkage porosity. The simulation provides us with results about the solidification time and the maximum temperature gradient at each junction in the castings. Then, we can determine the % limiting value of the thermal gradient and correlate the volume of shrinkage porosity in the real experiments with the simulation results. Subsequently, it becomes straightforward to compute the limiting value of the thermal gradient and the cooling rate using equations 1 and 2:

$$\begin{aligned} \text{Limiting value of thermal gradient (G)} &= \\ \text{Thermal gradient max} * & \\ \text{(limiting value of thermal gradient\%)} & \end{aligned} \tag{1}$$

$$\begin{aligned} \text{Cooling rate (r)} &= \\ \text{(pouring temperature – solidus temperature) /} & \\ \text{Solidification time} & \end{aligned} \tag{2}$$

The curve fitting method was used to establish the correlation between the limiting value of the thermal gradient and the thickness ratio. This aids in calculating the limiting thermal gradient values for various thickness ratio variations in benchmark castings, as represented by equations 3, 4, and 5.

First junction:
 $G = -1.523R_1^3 + 3.534R_1^2 - 1.370R_1 + 0.288$ (3)
 Second junction:

$$G = 3.215R_1^3 - 10.21R_1^2 + 9.900R_1 - 1.872 \quad (4)$$

Third junction:

$$G = -0.373R_1^3 + 1.088R_1^2 - 0.687R_1 + 0.154 \quad (5)$$

6. Development model of criterion function

It is necessary to generate more data to acquire sufficient information for creating a criterion function to predict shrinkage porosity. For this purpose, the number of thickness ratios has been increased, ranging from 0.25 to 1.5 with a step of 0.05 (the stem thickness is incremented by 1 mm with each change) for each T-junction while maintaining the same length ratio at 2, 3, and 4. This results in 26 different thickness ratios (R_1) variations corresponding to each length ratio (R_2), totaling 78 variations.

The criterion function to be developed in this study will encompass both thermal and geometrical effects. The variables considered within this criterion include the limiting value of thermal gradient, as well as length and thickness ratios, and cooling rate. The limiting value of the thermal gradient was calculated using equations 3, 4, and 5 for all 78 variations. The limiting value of the thermal gradient is related to the maximum thermal gradient, and this relationship determines the % limiting value of the gradient. A simulation of the solidification process was conducted, and the % limiting gradient and thickness ratio values were input into a simulation tool to obtain the shrinkage porosity. Information regarding the cooling rate was also obtained from the simulation. The results for the first junction are presented in Table 6.

Table 6. The resulting data for developing the criterion function related to the first junction.

| No. | Thickness ratio (R_1) | Length ratio (R_2) | Limiting value of thermal gradient (G) [$^{\circ}$ C/mm] | Thermal gradient max (G_{max}) [$^{\circ}$ C/mm] | % limiting value of thermal gradient (% G) | Cooling rate (r) [$^{\circ}$ C/sec] | Shrinkage porosity (P) [cm^3] |
|-----|---------------------------|------------------------|---|---|--|--------------------------------------|-----------------------------------|
| 1 | 0.25 | 2 | 0.14 | 12.44 | 1.15 | 1.32 | 0.10 |
| 2 | 0.30 | 2 | 0.15 | 12.44 | 1.24 | 1.32 | 0.10 |
| 3 | 0.35 | 2 | 0.18 | 12.44 | 1.42 | 1.32 | 0.12 |
| 4 | 0.40 | 2 | 0.21 | 12.44 | 1.67 | 1.32 | 0.11 |
| 5 | 0.45 | 2 | 0.25 | 12.44 | 2.00 | 1.32 | 0.12 |
| 6 | 0.50 | 2 | 0.30 | 12.30 | 2.41 | 1.22 | 0.21 |
| 7 | 0.55 | 2 | 0.35 | 12.20 | 2.87 | 1.14 | 0.27 |
| 8 | 0.60 | 2 | 0.41 | 12.13 | 3.37 | 1.06 | 0.36 |
| 9 | 0.65 | 2 | 0.47 | 12.09 | 3.91 | 1.00 | 0.43 |
| 10 | 0.70 | 2 | 0.54 | 12.06 | 4.46 | 0.94 | 0.49 |
| 11 | 0.75 | 2 | 0.61 | 12.05 | 5.03 | 0.88 | 0.56 |
| 12 | 0.80 | 2 | 0.67 | 12.05 | 5.59 | 0.84 | 0.57 |
| 13 | 0.85 | 2 | 0.74 | 11.97 | 6.19 | 0.76 | 0.70 |
| 14 | 0.90 | 2 | 0.81 | 11.69 | 6.91 | 0.73 | 0.85 |
| 15 | 0.95 | 2 | 0.87 | 11.42 | 7.62 | 0.70 | 1.18 |
| 16 | 1.00 | 2 | 0.93 | 11.18 | 8.31 | 0.67 | 1.59 |
| 17 | 1.05 | 2 | 0.98 | 10.96 | 8.97 | 0.65 | 1.81 |
| 18 | 1.10 | 2 | 1.03 | 10.76 | 9.57 | 0.63 | 2.11 |
| 19 | 1.15 | 2 | 1.07 | 10.61 | 10.08 | 0.63 | 2.36 |
| 20 | 1.20 | 2 | 1.10 | 10.51 | 10.48 | 0.59 | 2.46 |
| 21 | 1.25 | 2 | 1.12 | 10.42 | 10.78 | 0.57 | 2.89 |
| 22 | 1.30 | 2 | 1.13 | 10.34 | 10.96 | 0.55 | 2.98 |
| 23 | 1.35 | 2 | 1.13 | 10.54 | 10.74 | 0.54 | 2.83 |
| 24 | 1.40 | 2 | 1.12 | 10.45 | 10.69 | 0.52 | 2.93 |
| 25 | 1.45 | 2 | 1.09 | 10.37 | 10.50 | 0.51 | 2.76 |
| 26 | 1.50 | 2 | 1.04 | 10.34 | 10.10 | 0.50 | 2.51 |

The resulting data are utilized in developing a quantitative prediction model through the multiple regression technique, considering the geometrical factor, to predict the quantity of shrinkage porosity. In Table 7, it can be observed that the developed regression model is well-fitted, as evidenced by the high R-square (0.955) and adjusted R-square (0.938) values. The satisfactory range of t-stat and p-values for the limiting thermal gradient value, as well as length and thickness ratios and cooling rate, further supports the model's reliability. The low p-values highlight the significance of every factor in the quantitative prediction model, with the limiting value of thermal gradient (G) being the most important,

followed by thickness ratio (R_1), cooling rate (r), and length ratio (R_2). Equation (6) showcases the developed geometry-driven criterion function.

Table 7. Summary Report of Regression Analysis.

| | | | | |
|----------------|--------------|-------------|--------------|--------------|
| R Square | 0.955 | | | |
| R Square (adj) | 0.938 | | | |
| | ln (R_1) | ln(R_2) | ln(G) | ln(r) |
| Coefficients | -1.381 | 0.215 | 1.913 | -1.675 |
| t Stat | -5.882 | 1.580 | 28.482 | -4.697 |
| P-value | 1.47783 e-07 | 0.118796482 | 8.49336 e-39 | 1.38352 e-05 |

$$\%P = \frac{G^{1.913} \cdot R_2^{0.215}}{r^{1.675} \cdot R_1^{1.282}} \quad (6)$$

Where: G: Limiting value of thermal gradient, R_1 : Thickness ratio, r: Cooling rate, R_2 : Length ratio, %P: The volume of shrinkage porosity expressed as a percentage of the total casting volume.

7. Validation

To verify the validity of the developed criterion function, an experiment was carried out on a casting with thickness and length ratios of 1.75 and 5, respectively. The shrinkage porosity measured in this experiment was approximately 2.5 cm^3 (ml of water). Subsequently, this case was simulated, and the volume of shrinkage porosity was predicted using the developed criterion function by correlating the data obtained from this simulation, which includes parameters such as cooling rate and maximum temperature gradient, with real experimental data. The predicted shrinkage porosity volume from the developed function was 2.64 cm^3 , indicating a high accuracy of approximately 95%. Figure 5 presents a cross-section of the plain carbon steel casting utilized in this experiment to validate the T-joint casting.



Figure 5. Cross-section of Plain Carbon Steel Casting for T-Junction Validation.

8. Conclusion

The study focuses on developing a geometry-based quantitative prediction model for shrinkage porosity for T-junction steel sand castings. Casting of the designed benchmark shape and analysis of porosity formation reveal the significant influence of the presence of joints on shrinkage porosity. Correlating the experimental data with a simulation tool and generating more data by simulating castings of varying thickness ratios helped develop a more reliable criterion function. The resulting criterion function considers the influence of thermal and geometric factors simultaneously, enabling designers to utilize these data when planning experiments to prevent shrinkage porosity. The developed criterion function could help enhance the casting simulation tools already

in use for estimating shrinkage porosity in Plain Carbon Steel castings with T connections.

Author contributions

Kamar Mazloum: Writing, simulations, **Amit Sata:** Conceptualization, final editing, analysis.

Conflicts of interest

The authors declare no conflicts of interest.

References

1. Ramani, J., Dandge, S., & Chakraborty, S. (2020, November). Machinability study of plain carbon steels using data mining technique. In *AIP Conference Proceedings* (Vol. 2273, No. 1). AIP Publishing. <https://doi.org/10.1063/5.0024334>
2. Uzorh, A. C. (2013). Corrosion properties of plain carbon steels. *The International Journal of Engineering and Science*, 2(11), 18-24.
3. Couper, M. J., Neeson, A. E., & Griffiths, J. R. (1990). Casting defects and the fatigue behaviour of an aluminium casting alloy. *Fatigue & Fracture of Engineering Materials & Structures*, 13(3), 213-227.
4. Wang, Q. G., Apelian, D., & Lados, D. A. (2001). Fatigue behavior of A356-T6 aluminum cast alloys. Part I. Effect of casting defects. *Journal of Light Metals*, 1(1), 73-84. [https://doi.org/10.1016/S1471-5317\(00\)00008-0](https://doi.org/10.1016/S1471-5317(00)00008-0)
5. Hardin, R. A., & Beckermann, C. (2013). Effect of porosity on deformation, damage, and fracture of cast steel. *Metallurgical and Materials Transactions A*, 44, 5316-5332. <https://doi.org/10.1007/s11661-013-1669-z>
6. Xu, Z., Wang, X., & Jiang, M. (2017). Investigation on improvement of center porosity with heavy reduction in continuously cast thick slabs. *Steel Research International*, 88(2), 1600061. <https://doi.org/10.1002/srin.201600061>
7. Yao, R. Q., & Tang, H. Q. (2011). The numerical simulation and optimization of squeeze casting process for producing magnesium wheels. *Advanced Materials Research*, 299, 955-961. <https://doi.org/10.4028/www.scientific.net/AMR.299-300.955>
8. Kuang, W., Wang, H., Li, X., Zhang, J., Zhou, Q., & Zhao, Y. (2018). Application of the thermodynamic extremal principle to diffusion-controlled phase transformations in Fe-CX alloys: Modeling and applications. *Acta Materialia*, 159, 16-30. <https://doi.org/10.1016/j.actamat.2018.08.008>
9. Chen, L., Zhao, Y., Yan, F., & Hou, H. (2017). Statistical investigations of serpentine channel pouring process parameters on semi-solid ZL101 aluminum alloy slurry using response surface methodology. *Journal of Alloys and Compounds*, 725, 673-683. <https://doi.org/10.1016/j.jallcom.2017.07.169>
10. Zhao, P., Dong, Z., Zhang, J., Zhang, Y., Cao, M., Zhu, Z., ... & Fu, J. (2020). Optimization of injection-molding process parameters for weight control: converting optimization problem to classification problem.

- Advances in Polymer Technology*, 2020, 1-9. <https://doi.org/10.1155/2020/7654249>
11. Cao, L., Liao, D., Sun, F., Chen, T., Teng, Z., & Tang, Y. (2018). Prediction of gas entrapment defects during zinc alloy high-pressure die casting based on gas-liquid multiphase flow model. *The International Journal of Advanced Manufacturing Technology*, 94, 807-815. <https://doi.org/10.1007/s00170-017-0926-5>
 12. Shafyei, A., Anijdan, S. M., & Bahrami, A. (2006). Prediction of porosity percent in Al-Si casting alloys using ANN. *Materials Science and Engineering: A*, 431(1-2), 206-210. <https://doi.org/10.1016/j.msea.2006.05.150>
 13. Kumruoglu, L. C., & Özer, A. (2008). Investigation of critical liquid fraction factor in nodular iron castings by computer simulation. *Journal of Materials Processing Technology*, 197(1-3), 182-188. <https://doi.org/10.1016/j.jmatprotec.2007.06.008>
 14. Rathod, H., Dhulia, J. K., & Maniar, N. P. (2017, August). Prediction of shrinkage porosity defect in sand casting process of LM25. In *IOP Conference Series: Materials Science and Engineering* (Vol. 225, No. 1, p. 012237). IOP Publishing. <https://doi.org/10.1088/1757-899X/225/1/012237>
 15. Chen, Z., Li, Y., Zhao, F., Li, S., & Zhang, J. (2022). Progress in numerical simulation of casting process. *Measurement and Control*, 55(5-6), 257-264. <https://doi.org/10.1177/00202940221102656>
 16. Cemernek, D., Cemernek, S., Gursch, H., Pandeshwar, A., Leitner, T., Berger, M., ... & Kern, R. (2021). Machine learning in continuous casting of steel: A state-of-the-art survey. *Journal of Intelligent Manufacturing*, 1-19. <https://doi.org/10.1007/s10845-021-01754-7>
 17. Kubo, K., & Pehlke, R. D. (1985). Mathematical modeling of porosity formation in solidification. *Metallurgical Transactions B*, 16, 359-366. <https://doi.org/10.1007/BF02679728>
 18. Saleh, S. M., & İhsan, A. A. (2021). Strength and behaviour assessment of axially loaded concrete filled steel tubular stub columns. *Turkish Journal of Engineering*, 5(4), 154-164. <https://doi.org/10.31127/tuje.686246>
 19. Chen, Y. H., & Im, Y. T. (1990). Analysis of solidification in sand and permanent mold castings and shrinkage prediction. *International Journal of Machine Tools and Manufacture*, 30(2), 175-189. [https://doi.org/10.1016/0890-6955\(90\)90128-6](https://doi.org/10.1016/0890-6955(90)90128-6)
 20. Inegbedion, F., & James, O. R. J. I. (2023). Determination of the critical drop height and critical flow velocity of aluminum alloy (AL-91% Mg-8% Fe-0.4% Zn-0.2%) in gravity sand casting. *Turkish Journal of Engineering*, 7(2), 149-156. <https://doi.org/10.31127/tuje.1077467>
 21. Asan, Y. E., & Çolak, M. (2022). Modeling the effect of pour height, casting temperature and die preheating temperature on the fluidity of different section thicknesses in permanent mold casting of Al12Si alloys. *Erzincan University Journal of Science and Technology*, 15(Special Issue I), 14-27. <https://doi.org/10.18185/erzifbed.1199648>
 22. Sabau, A. S., & Viswanathan, S. (2002). Microporosity prediction in aluminum alloy castings. *Metallurgical and Materials Transactions B*, 33, 243-255. <https://doi.org/10.1007/s11663-002-0009-2>
 23. Pequet, C., Rappaz, M., & Gremaud, M. (2002). Modeling of microporosity, macroporosity, and pipe-shrinkage formation during the solidification of alloys using a mushy-zone refinement method: Applications to aluminum alloys. *Metallurgical and Materials Transactions A*, 33, 2095-2106. <https://doi.org/10.1007/s11661-002-0041-5>
 24. Sun, D., & Garimella, S. V. (2007). Numerical and experimental investigation of solidification shrinkage. *Numerical Heat Transfer, Part A: Applications*, 52(2), 145-162. <https://doi.org/10.1080/10407780601115079>
 25. de Obaldia, E. E., & Felicelli, S. D. (2007). Quantitative prediction of microporosity in aluminum alloys. *Journal of Materials Processing Technology*, 191(1-3), 265-269. <https://doi.org/10.1016/j.jmatprotec.2007.03.072>
 26. Reis, A., Houbaert, Y., Xu, Z., Van Tol, R., Santos, A. D., Duarte, J. F., & Magalhaes, A. B. (2008). Modeling of shrinkage defects during solidification of long and short freezing materials. *Journal of Materials Processing Technology*, 202(1-3), 428-434. <https://doi.org/10.1016/j.jmatprotec.2007.10.030>
 27. Tavakoli, R. (2014). On the prediction of shrinkage defects by thermal criterion functions. *The International Journal of Advanced Manufacturing Technology*, 74, 569-579. <https://doi.org/10.1007/s00170-014-5995-0>
 28. Sutaria, M. (2013). Casting solidification feed-paths: Modeling, computation and applications (Doctoral thesis). *Indian Institute of Technology Bombay*.
 29. ASM. (1962). *Casting design handbook*. American Society of Metals.
 30. Noda, N. A., Egawa, S., Tashiro, Y., & Takenouchi, K. (2009). Predicting locations of defects in the solidification process for large-scale cast steel. *Journal of Computational Science and Technology*, 3(1), 242-251. <https://doi.org/10.1299/JCST.3.242>
 31. Joshi, D., & Ravi, B. (2009). Classification and simulation-based design of 3D junctions in castings. *AFS Transactions*, 117, 7-22.
 32. Kabnure, B. B., Shinde, V. D., & Patil, D. C. (2020). Quality and yield improvement of ductile iron casting by simulation technique. *Materials Today: Proceedings*, 27, 111-116. <https://doi.org/10.1016/j.matpr.2019.09.022>

